


Diagnosing first- and second-order phase transitions with probes of quantum chaos

Kyong-Bum Huh,^{1,*} Kazuki Ikeda,^{2,†} Viktor Jahnke^{1,‡} and Keun-Young Kim^{1,§}

¹*School of Physics and Chemistry, Gwangju Institute of Science and Technology, Gwangju 61005, Korea*

²*Department of Physics, Osaka University, Toyonaka, Osaka 5600043, Japan*

 (Received 13 January 2021; revised 17 June 2021; accepted 6 July 2021; published 27 August 2021)

We explore quantum phase transitions using two probes of quantum chaos: out-of-time-order correlators (OTOCs) and the r -parameter obtained from the level spacing statistics. In particular, we address p -spin models associated with quantum annealing or reverse annealing. Quantum annealing triggers first-order or second-order phase transitions, which is crucial for the performance of quantum devices. We find that the time-averaging OTOCs for the ground state and the average r -parameter change behavior around the corresponding transition points, diagnosing the phase transition. Furthermore, they can identify the order (first or second) of the phase transition by their behavior at the quantum transition point, which changes abruptly (smoothly) in the case of first-order (second-order) phase transitions.

DOI: [10.1103/PhysRevE.104.024136](https://doi.org/10.1103/PhysRevE.104.024136)

I. INTRODUCTION

In recent years, out-of-time-order correlators (OTOCs) [1] have gained renewed interest, especially because of their connection with many-body quantum chaos, black hole physics, and holography [2,3]. Such developments in the holographic description of quantum chaos were recently reviewed in [4]. For works regarding the experimental measurement of OTOCs, we refer to [5–8].

An OTOC is defined as

$$F_{VW}(t) = \langle W(t)V(0)W(t)V(0) \rangle, \quad (1)$$

where V and W are some simple operators and the expectation value is usually taken in a thermal state. The idea is that chaotic behavior leads to an early-time exponential¹ suppression and the late-time vanishing of OTOCs, which happens for almost any choice of operators V and W . On the other hand, the absence of chaos is expected to result in a nonuniversal, operator-dependent behavior of $F_{VW}(t)$.

Another way to characterize quantum chaotic behavior is through the statistics of the spacing between consecutive energy eigenvalues, which is usually known as *level spacing statistics*. In chaotic systems, the level spacing statistics obeys a Wigner-Dyson distribution [9], while in integrable systems, it follows a Poisson distribution [10,11]. We can also study the so-called r -parameter statistics, which is computed from the level spacing information. The average r -parameter takes different values depending on whether the system is chaotic or integrable. We discuss the level spacing and the r -parameter statistics in more detail in Sec. IV.

The level spacing statistics is defined at zero temperature and involves timescales much bigger than the ones involved in the behavior of OTOCs, which are usually computed at finite temperature. Despite these differences, both the level spacing statistics and the OTOCs can probe chaotic behavior, presumably capturing different aspects of it, due to the thermal nature of OTOCs.

Thermal effects can be removed by considering ground-state OTOCs, in which the expectation value is taken in the ground state of the system. In this case, the OTOCs are completely controlled by the ground-state physics [12] and may become sensitive to changes in the ground state, i.e., they may diagnose quantum phase transitions [12–14]. On the other hand, the level spacing statistics is known to be sensitive to phase transitions, being able to detect, for example, metal-insulator transitions in the Anderson model [15,16] or Hawking-Page-like transitions in the mass deformed Sachdev-Ye-Kitaev model [17–19]. One of the goals of this paper is to use the statistics of level spacing ratios to study a particular type of phase transition and clarify the role played by chaos in the process.

Quantum phase transitions are transitions between different phases of matter that occur at zero temperature by variation of a nonthermal control parameter. Quantum phase transitions have found applications in the description of several properties of condensed matter systems [20] as well as in quantum computation algorithms. In this work, we will be interested in quantum phase transitions that are triggered by a method of adiabatic quantum computation known as *quantum annealing*.

Quantum annealing [21] is a metaheuristic quantum method for solving combinatorial optimization problems and could be as powerful as universal computation when a system with a nonstoquastic Hamiltonian evolves in an adiabatic way [22]. The conventional form of quantum annealing is done by the quantum mechanical time evolution of an initial state, which is the ground state of a transverse magnetic field. The initial phase consists of the uniform superposition of all

*hkabell1689@gist.ac.kr

†kazuki7131@gmail.com

‡viktorjahnke@gist.ac.kr

§fortoe@gist.ac.kr

¹See Sec. III A for subtleties and clarifications about the exponential behavior.

possible classical states, which is called the quantum paramagnetic (QP) phase. In general, the system evolves into a different phase and the performance of a quantum annealer depends heavily on the choice of transition paths. According to the adiabatic theorem, the computational time that is needed to efficiently obtain the ground state is proportional to the inverse square of the minimal energy gap Δ between the ground state and the first-excited state. A lot of examples indicate that Δ decays polynomially if a phase transition is second order [23,24], whereas Δ decays exponentially if it is first order (although there are some exceptions [25–27]). Therefore, the problem in the case of systems with second-order phase transitions is efficiently solved. There are some models for which the first-order phase transitions can be avoided when a nonstoquastic Hamiltonian or reverse annealing [28] is used. The p -spin model we address in this article is a typical example (see, also, [29,30]). The ground state of the p -spin model is ferromagnetic (F) and, depending on the path, the QP-F transition becomes first order or second order. In [29,31], it is suggested that entanglement measures are good tools to analyze phase transitions of such a fully connected spin system.

In this work, we aim at diagnosing quantum phase transitions triggered by quantum annealing using two probes of quantum chaos, namely, OTOCs and the r -parameter statistics. The relation between phase transitions and the time average of OTOCs was first reported in [32], which observed that ground-state OTOCs constructed out of magnetization operators can diagnose second-order phase transitions in Ising chains. The effectiveness of ground-state OTOCs in detecting phase transitions was partially elucidated in [12], which showed that ground-state OTOCs are dominated by the ground-state physics, which also controls phase transitions. Some other developments exploring the relation between phase transitions and OTOCs include, for instance, those in Refs. [12–14,33–35]. The above results suggest that OTOCs can be used as order parameters to characterize phase transitions. It is not clear, however, whether generic OTOCs made out of local operators can also diagnose phase transitions in more general systems. In addition, less is known about the relation between the order of the phase transition and the behavior of OTOCs, including the relation between phase transitions and the average r -parameter. In this paper, we show that OTOCs (including the ones made out of local operators) and the average r -parameter not only detect the phase transition, but also distinguish the order of the phase transition. Our paper includes the following aspects: (1) relating both first-order and second-order phase transitions with the dynamics of OTOCs and the r -parameter statistics; (2) using probes of quantum chaos to study quantum annealing or adiabatic quantum computing; and (3) the Hamiltonians we employed are nonstoquastic, which means the models cannot be efficiently simulated using classical ways. Some stoquastic models are studied elsewhere [12,32–35].

This article is organized as follows. In Sec. II, we review and explain the phase transition associated with quantum annealing of the p -spin model. In Sec. III, we use the time average of OTOCs to characterize the QP-F transition. In Sec. IV, we study the r -parameter statistics and show that the average r -parameter is sensitive to the phase transition. In

Sec. V, we address phase transitions associated with reverse annealing and provide more evidence that they can be diagnosed by the time average of OTOCs. Finally, we present our conclusions in Sec. VI.

II. MODEL

Let us start with a Hamiltonian of adiabatic quantum computation,

$$H(s) = sH_T + (1-s)H_I, \quad s \in [0, 1], \quad (2)$$

where H_T is a target Hamiltonian and H_I is an initial Hamiltonian. They should not commute, $[H_I, H_T] \neq 0$. As an initial Hamiltonian, we use the widely used transverse magnetic field [21,22],

$$H_I = -\sum_i^N X_i, \quad (3)$$

and as a target Hamiltonian, let us consider the Hamiltonian of the p -spin model,

$$H_T = -N \left(\frac{1}{N} \sum_{i=1}^N Z_i \right)^p, \quad (4)$$

where X_i and Z_i denote, for example,

$$\begin{aligned} X_1 &= \sigma_x \otimes I_2 \otimes I_2 \otimes \cdots \otimes I_2, \\ Z_3 &= I_2 \otimes I_2 \otimes \sigma_z \otimes I_2 \otimes \cdots \otimes I_2, \end{aligned} \quad (5)$$

with $\sigma_x = \begin{pmatrix} 0 & 1 \\ 1 & 0 \end{pmatrix}$, $\sigma_z = \begin{pmatrix} 1 & 0 \\ 0 & -1 \end{pmatrix}$.

The Hamiltonian (2) is stoquastic. We say a Hamiltonian is stoquastic if all off-diagonal matrix elements in the standard basis are real and nonpositive; otherwise, it is nonstoquastic [36]. We add a term that introduces nonstoquastic antiferromagnetic (AF) interactions,

$$H_{AF} = +N \left(\frac{1}{N} \sum_i^N X_i \right)^2, \quad (6)$$

in such a way that

$$H(s, \lambda) = s[\lambda H_T + (1-\lambda)H_{AF}] + (1-s)H_I. \quad (7)$$

Even though a nonstoquastic term is, in general, hard to simulate by quantum Monte Carlo due to the negative sign problem, sometimes it makes problems efficiently solvable by adiabatic quantum computation or quantum annealing [37]. Furthermore, it is believed that adding a stoquastic Hamiltonian to (2) is not helpful for quantum speedup.

The initial Hamiltonian ($s = 0$) is $H(0, \lambda) = H_I$ with any λ . The final Hamiltonian is chosen to be $H(1, 1) = H_T$. At the initial stage of annealing ($s = 0$), since $\sigma_x |+\rangle_i = |+\rangle_i$, the ground state $|\psi_{QP}\rangle$ is a superposition of all possible 2^N states with an equal probability weight,

$$\begin{aligned} |\psi_{QP}\rangle := \prod_i^N |+\rangle_i &= \frac{1}{\sqrt{2^N}} (|\uparrow\uparrow \cdots \uparrow\rangle + |\uparrow\uparrow \cdots \uparrow\downarrow\rangle + \cdots \\ &+ |\downarrow\downarrow \cdots \downarrow\rangle), \end{aligned} \quad (8)$$

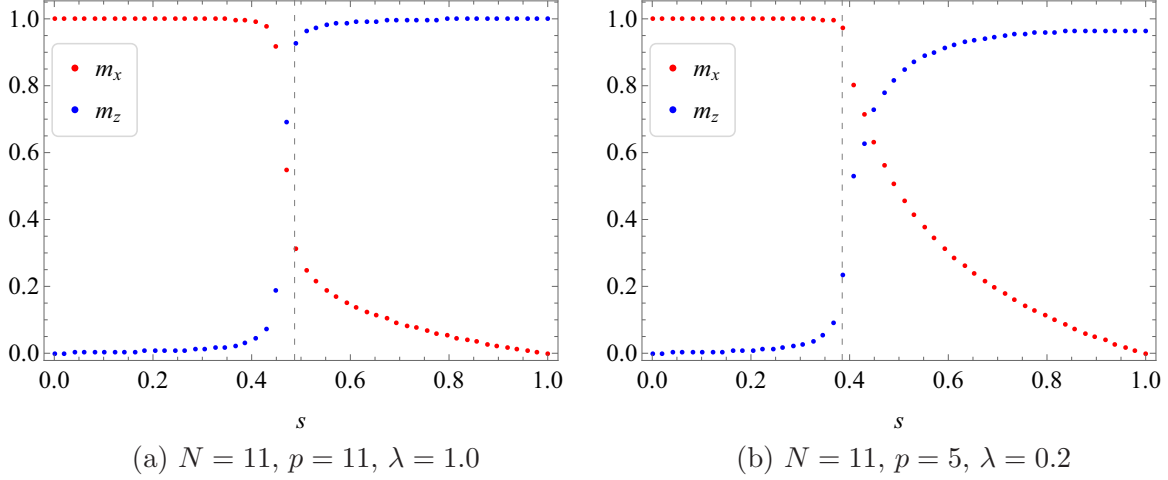


FIG. 1. Magnetizations m_x and m_z vs s for $N = 11$. There are the (a) first-order or (b) second-order phase transitions between the QP phase (8) and the F phase (9). The vertical dashed line indicates the transition point.

which we call the quantum paramagnetic (QP) phase. Here, $|\uparrow\rangle$ and $|\downarrow\rangle$ denote eigenstates of σ_z at each site, i.e., $\sigma_z |\uparrow\rangle_i = |\uparrow\rangle_i$ and $\sigma_z |\downarrow\rangle_i = -|\downarrow\rangle_i$.

The ground state of the target Hamiltonian H_T is degenerated if p is even so we consider the cases when p is odd. Then the ground state of H_T consists of all spins pointing up,

$$|\psi_F\rangle := |\uparrow\uparrow\cdots\uparrow\rangle, \quad (9)$$

which is the ferromagnetic (F) phase.

Hence, as s increases, a phase transition from the QP phase to the F phase occurs. The corresponding order parameters are magnetizations,

$$m_x := \frac{1}{N} \sum_i \langle X_i \rangle, \quad m_z := \frac{1}{N} \sum_i \langle Z_i \rangle, \quad (10)$$

where the expectation value is obtained by the ground state at a given s . The first-order (second-order) phase transitions are defined by the discontinuity (continuity) of a given order parameter, respectively. Without the antiferromagnetic interactions ($\lambda = 1$), it is known that this model costs an exponentially long time to obtain the ground state of H_T due to a first-order phase transition [38]. The first-order phase transition can be avoided by strong enough antiferromagnetic interactions, with which the problem can be solved efficiently [29,37,39]. In fact, by studying the behavior of m_x along the quantum annealing process, the authors of [37] showed that for $p > 3$, the system displays a first-order phase transition when $\lambda \gtrsim 0.4$, but the transition becomes second order for smaller values of λ . In their analysis, they consider a large- N approximation. This phase transition was also studied at large N using a spin-coherent state technique [29], which gives results that are consistent with the analysis of [37].

In this section, we first reproduce some of the results of [37] at finite N without using a large- N approximation. By performing a direct diagonalization of the Hamiltonian (7), we numerically compute the ground-state expectation values in (10). This is an important step because we will compute OTOCs at finite N in the subsequent sections and try to un-

derstand its large- N properties. Thus, we first need to find an optimal N which can be taken as large enough with reasonable computing time.

Figure 1 shows the behavior of the magnetizations m_x and m_z as functions of s for some values of N , λ , and p . As expected, at $s = 0$, m_x (m_z) starts from one (zero) and decreases (increases) to zero (a constant positive value) as we increase s . We chose $N = 11$ for the sake of comparison because it is the optimal value that we will use in the following OTOC computation. If $\lambda \gtrsim 0.4$, the transition is first order, while if $\lambda \lesssim 0.4$, the transition is second order. To show this, we choose $\lambda = 0.2$ and $\lambda = 1$. The feature of the first-order phase transition can be seen with $N = 11$ in Fig. 1(a), but it is clearer for larger values of N . See Fig. 2, where we set $N = 20$.

III. DIAGNOSING QUANTUM PHASE TRANSITION WITH OTOC

In the previous section, we reviewed that the system described by the Hamiltonian (7) displays a quantum phase transition from a quantum paramagnetic (QP) phase to a ferromagnetic (F) phase as we change the parameter s from 0 to 1. In this section, we study quantum phase transitions from the viewpoint of quantum chaos, in particular in terms of out-of-time-order correlators (OTOCs).

A. Short review of OTOCs

Here we provide a short review of OTOCs. For more details, we refer the reader to [4].² OTOCs have the form

$$F_{VW}(t) = \langle W(t)VW(t)V \rangle, \quad (11)$$

where V and W are Hermitian and unitary local operators. In chaotic many-body systems, one expects $F_{VW}(t)$ to vanish at late times for almost any choice of operators V and W .

²For recent applications in the context of holographic duality, see [40,41] and references therein.

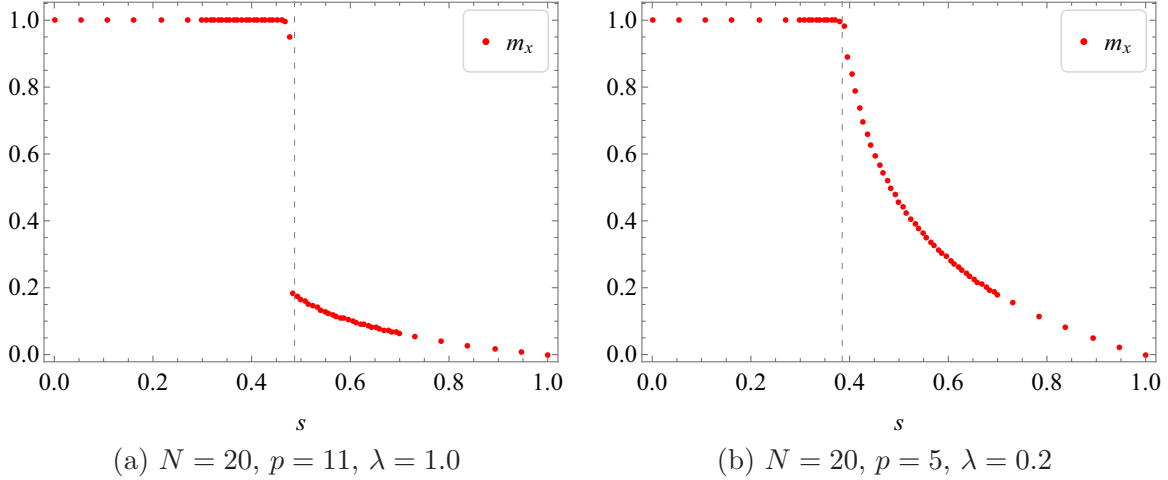


FIG. 2. Magnetization m_x vs s for $N = 20$. There are the (a) first-order or (b) second-order transitions between the QP phase (8) and the F phase (9). The first-order phase transition is clearer when compared to Fig. 1(a), where we set $N = 11$. The vertical dashed line indicates the transition point.

The late-time vanishing of OTOCs is tied to the idea of scrambling of quantum information, which takes place in chaotic systems. Using the Baker-Campbell-Hausdorff (BCH) formula, we can write the Heisenberg operator as

$$\begin{aligned} W(t) &= e^{iHt} W e^{-iHt} \\ &= W + it [H, W] + \frac{(it)^2}{2!} [H, [H, W]] + \dots \end{aligned} \quad (12)$$

At $t = 0$, the operator only involves the local degrees of freedom associated with W . Under time evolution, higher-order terms in the BCH become important, and $W(t)$ becomes more and more complicated as it starts to act nontrivially in an increasing number of degrees of freedom. In other words, the operator $W(t)$ “grows” with time, and the initially local information gets scrambled into a nonlocal form.

The scrambling of the operator $W(t)$ can be probed by considering its commutator with some other, local operator V . To avoid phase cancellations, one usually defines the double commutator

$$C(t) = \langle |[W(t), V]|^2 \rangle, \quad (13)$$

which starts at zero and grows as $W(t)$ scrambles with an increasing number of degrees of freedom. After the so-called “scrambling time,” the operator $W(t)$ is scrambled with essentially all the degrees of freedom of the system, and $C(t)$ saturates to a constant value, which equals $2 \langle VV \rangle \langle WW \rangle$. The double commutator is closely related to OTOCs. For unitary V and W , the double commutator can be written as $C(t) = 2\{1 - \text{Re}[F_{VW}(t)]\}$. Hence, the saturation of the double commutator after the scrambling time implies the vanishing of OTOCs.³ In contrast, in nonchaotic systems, one expects a nonuniversal behavior of the OTOCs, which in general depends on the choice of the operators V and W . Moreover, the absence of

thermalization in integrable systems is expected to lead to an oscillatory behavior of OTOCs.

The way $F_{VW}(t)$ approaches zero is particularly simple in systems that display some sort of classical limit (e.g., quantum mechanical systems that have a well-defined $\hbar \rightarrow 0$ limit or certain large- N systems). In those cases, in an appropriate time window, the double commutator grows exponentially, i.e., $C(t) \sim e^{\lambda_L t}$, which is reminiscent of the divergence in the distance between initially nearby trajectories in the phase space of classically chaotic systems. In those cases, one can define a quantum Lyapunov exponent λ_L characterizing the onset of chaos in the system. By contrast, in standard spin chain models with local interactions, $F_{VW}(t)$ does not have any sort of exponential behavior with time [43,44], even for systems that are known to be strongly chaotic by other more conventional criteria for quantum chaos. This prevents the definition of a quantum Lyapunov exponent for those systems⁴ (see, however, [45]). Despite the absence of exponential behavior, one usually expects to distinguish chaotic and integrable systems by the late-time behavior of OTOCs, which vanishes in the case of many-body chaotic systems.

In the case of systems that are neither integrable nor chaotic (mixed systems), it has been proposed that the late-time oscillations of OTOCs can be used to characterize the degree of chaoticity, with the oscillation amplitudes being smaller and smaller for systems with increasing degrees of chaoticity [46]. We confirm these ideas in Appendix A by studying the behavior of OTOCs across an integrable-to-chaotic transition in a mixed field Ising chain.

In finite-size chaotic systems, OTOCs do not decay exactly to zero at late times. In fact, it has been shown that

³For an intuitive explanation (in the context of spin chains) of why the vanishing of OTOCs implies chaos, we refer the reader to [42]. See, also, Sec. 3 of [4].

⁴The timescale at which the OTOC vanishes is called the scrambling time t_* . If $C(t) \sim e^{\lambda_L t}$ at early times, then $t_* \sim \ln N_{\text{dof}}$, where N_{dof} is the number of degrees of freedom per site. For spin chains with local interactions, one typically has $t_* \sim O(1)$, which leaves no “room” for an exponential growth [43,44].

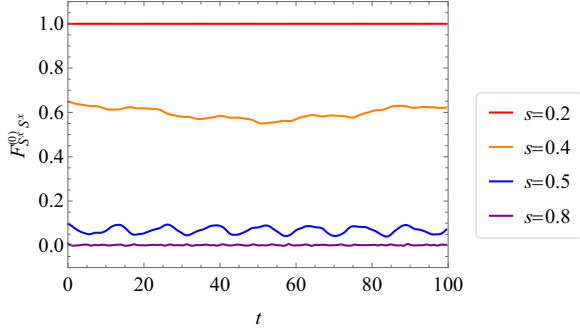


FIG. 3. Time dependence of $F_{S^x S^x}^{(0)}(t)$ for increasing values of the annealing parameter s . Here we set $N = 11$, $p = 5$, and $\lambda = 0.2$. The OTOC oscillates around a constant positive value that depends on the value of s .

the residual late-time value of OTOCs provides useful insights into the chaotic dynamics [42]. For energy-conserving chaotic spin chains, for example, the late-time value of the OTOCs scales as an inverse polynomial in the system size [42].

B. Ground-state OTOCs

We are interested in ground-state OTOCs,

$$F_{VW}^{(0)}(t) = \langle \phi_0 | W(t) V W(t) V | \phi_0 \rangle, \quad (14)$$

where V and W are Hermitian operators and $|\phi_0\rangle$ is the ground state of the total Hamiltonian $H = H(s, \lambda)$. In the following, we consider cases where V and W are nonlocal operators, such as

$$S^x = \frac{1}{2} \sum_{i=1}^N \sigma_i^x \quad \text{or} \quad S^z = \frac{1}{2} \sum_{i=1}^N \sigma_i^z, \quad (15)$$

and also cases where V and W are local unitary operators, such as X_i or Z_i , for some site i as in (5).

In both cases, the OTOCs show a qualitatively similar behavior, but the results for nonlocal operators tend to be

smoother. As an example, we show in Fig. 3 the time dependence of $F_{S^x S^x}^{(0)}(t)$ for increasing values of the annealing parameter s . In the beginning of the annealing process, when $s < s_c$ (in this case, $s_c = 0.385$) and the system is in the QP phase, $F_{S^x S^x}^{(0)}$ oscillates around one. After the phase transition to the F phase, for $s > s_c$, $F_{S^x S^x}^{(0)}$ oscillates around a constant (smaller than one) value that quickly decreases to zero as s approaches one.

The above time behavior indicates that the time-averaging OTOCs,

$$\bar{F}_{VW}^{(0)} = \lim_{T \rightarrow \infty} \frac{1}{T} \int_0^T F_{VW}^{(0)}(t) dt, \quad (16)$$

can diagnose the phase transition. We have checked that this is indeed true by studying the behavior of $\bar{F}_{VW}^{(0)}$ along the annealing process. Figure 4 shows the behavior of $\bar{F}_{S^x S^x}^{(0)}$ as a function of the annealing parameter s . The time-averaging OTOC changes behavior across the quantum phase transition, whose transition points (estimated at large N) are indicated in the plots by vertical lines. The transition points of the second-order phase transitions obey the formula $s_c = \frac{1}{3-2\lambda}$ and those of the first-order phase transitions are numerically estimated in [29]. Those estimates become more and more precise as we consider larger values of N .

The choice of parameters for Fig. 4 is such that we have a first-order phase transition in Fig. 4(a), where $(p, \lambda) = (11, 1)$, and a second-order phase transition in Fig. 4(b), where $(p, \lambda) = (5, 0.2)$. The order of the phase transition is visible in the behavior of the time-averaging OTOC, especially when we consider the curves for $N = 13$, where we can see that $\bar{F}_{S^x S^x}^{(0)}$ has a discontinuous (continuous) behavior at the quantum transition point in first-order (second-order) phase transitions.

The diagnosis of the phase transition in terms of time-averaging OTOCs is not limited to a particular choice of operators. Figure 5 shows that $\bar{F}_{S^z S^z}^{(0)}$ changes behavior around the quantum transition point and also identifies the order of the phase transition. The same is true for time-averaging OTOCs involving local operators, e.g., $\bar{F}_{X_i X_8}^{(0)}$, as is shown in Fig. 6. We have also checked that it is possible to

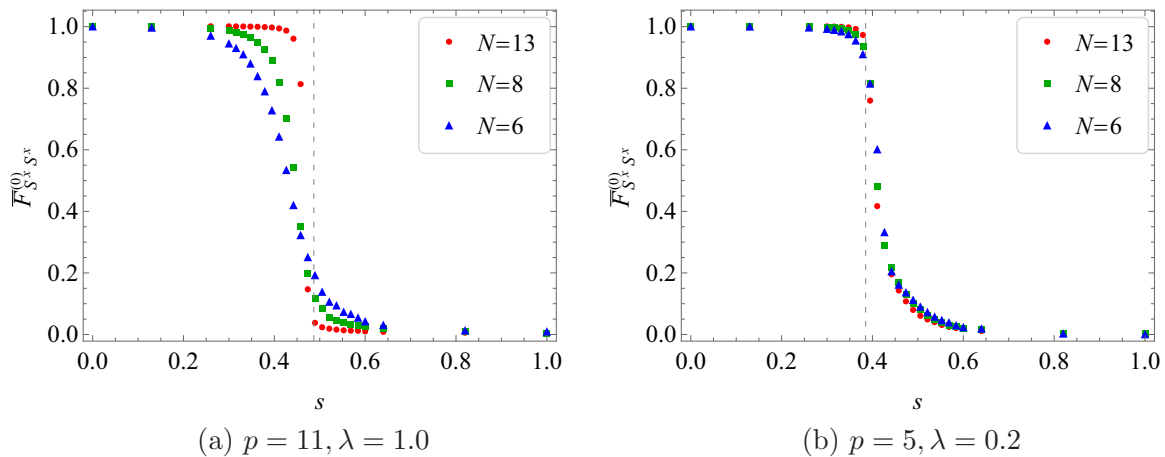


FIG. 4. Time-averaging OTOCs $\bar{F}_{S^x S^x}^{(0)}$ vs the annealing parameter s . Here we set $N = 6, 8, 13$. The phase transition is first order for $(p, \lambda) = (11, 1.0)$ and second order for $(p, \lambda) = (5, 0.2)$. The transition points of the second-order phase transitions obey the formula $s = \frac{1}{3-2\lambda}$ and those of the first-order phase transitions are numerically estimated in [29].

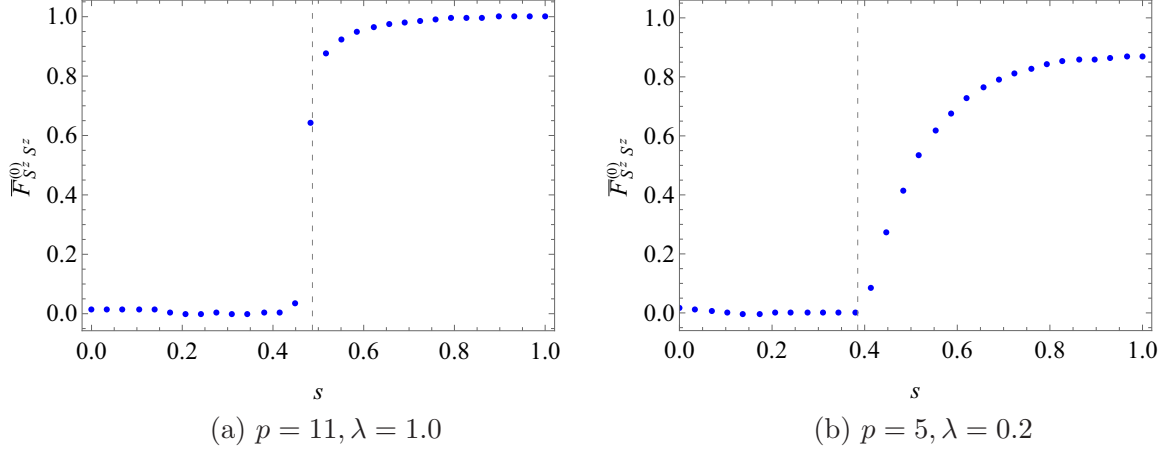


FIG. 5. Time-averaging OTOC $\bar{F}_{S^z S^z}^{(0)}$ vs the annealing parameter s . The transition points for each case are indicated by vertical lines. Here we set $N = 11$.

detect the phase transition with different combinations, such as $(V, W) = (Y_i, X_i), (X_i, Z_i)$, etc. In this sense, we may say that the OTOCs provide a generalization of the order parameter, and thereby are useful to characterize a phase transition when the rigorous order parameter is unknown.

Naively, the fact that $\bar{F}_{X_i X_8}^{(0)}$ is initially one in the QP phase, and zero in the F phase, seems to suggest that the F phase is chaotic, but this is not correct. In fact, time-averaging OTOCs of the form $\bar{F}_{Z_i Z_j}^{(0)}$ start at zero in the QP phase and approach one in the F phase; see Fig. 8(a). That means that the value that $\bar{F}_{VW}^{(0)}$ takes in each phase depends on the operators V and W in the corresponding OTOC. We understand this operator dependence of $\bar{F}_{VW}^{(0)}$ as due to the absence of scrambling in the ground-state OTOCs. As we will see in the next section, the system under consideration displays some degree of scrambling at finite temperature, which makes thermal OTOCs oscillate around zero at late times in both phases. However, as we reduce the temperature, the physics is dominated by the ground state and the behavior of $\bar{F}_{Z_i Z_j}^{(0)}$ and $\bar{F}_{X_i X_j}^{(0)}$ as a function of s starts to mimic the behavior of the magnetizations m_z and m_x , respectively.

C. Thermal OTOCs

We now consider thermal OTOCs to study thermal effects and the relation to chaos. Similarly to the ground-state OTOCs, we first study the time-averaging thermal OTOC,

$$\bar{F}_{S^x S^x}^\beta \equiv \lim_{T \rightarrow \infty} \frac{1}{T} \int_0^T F_{S^x S^x}^\beta(t) dt, \quad (17)$$

where

$$F_{S^x S^x}^\beta(t) \equiv \langle F_{S^x S^x}(t) \rangle_\beta \equiv \frac{\text{Tr}[e^{-\beta H} F_{S^x S^x}(t)]}{\text{Tr}[e^{-\beta H}]}, \quad (18)$$

with the inverse temperature β .

Figure 7 shows that the time-averaging thermal OTOC $\bar{F}_{S^x S^x}^\beta$ can successfully diagnose the phase transition at small temperatures, as expected. In high-temperature regimes, $\bar{F}_{S^x S^x}^\beta$ vanishes in both phases. At small temperatures, thermal OTOCs are dominated by a contribution coming from the ground state, and contributions from higher excited states are exponentially suppressed. In fact, if $\mathcal{F}(t) =$

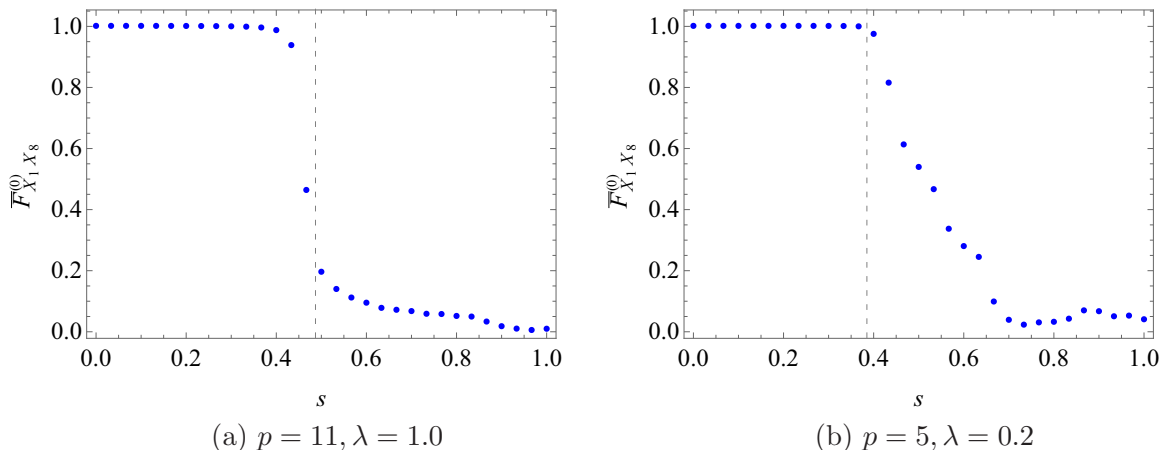


FIG. 6. Time-averaging OTOC $\bar{F}_{X_i X_8}^{(0)}$ vs the annealing parameter s . The transition points for each case are indicated by vertical lines. Here we set $N = 11$.

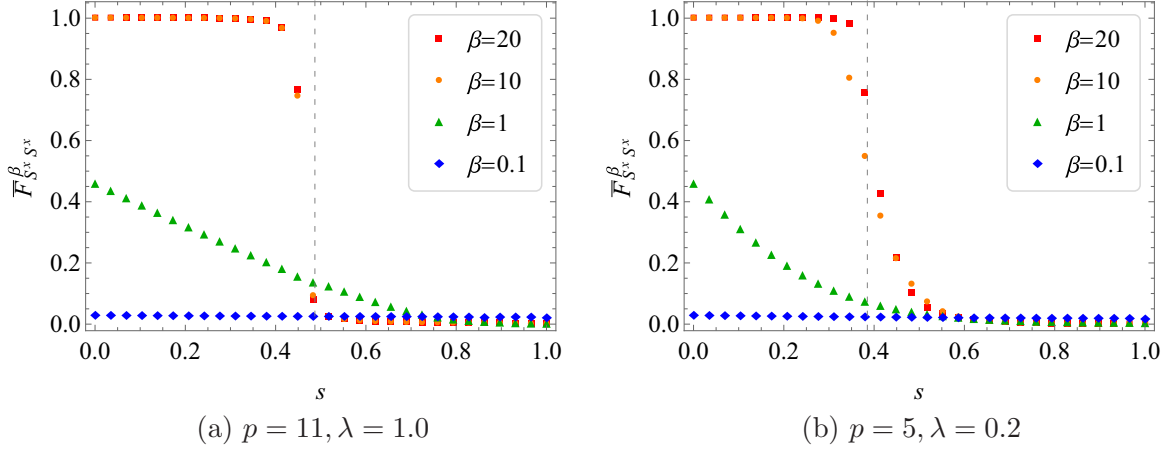


FIG. 7. Time average of the thermal OTOC $\bar{F}_{S^x S^x}^\beta$ vs the annealing parameter s . The transition points for each case are indicated by vertical lines. We set $N = 11$. β is the inverse temperature.

$W(t)V(0)W(t)V(0)$, we can write

$$\begin{aligned} \langle \mathcal{F}(t) \rangle_\beta &= \frac{\text{Tr}[e^{-\beta H} \mathcal{F}(t)]}{\text{Tr}[e^{-\beta H}]} = \frac{\sum_{n=0}^{\infty} e^{-\beta E_n} \langle n | \mathcal{F}(t) | n \rangle}{\sum_{n=0}^{\infty} e^{-\beta E_n}} \\ &= \langle 0 | \mathcal{F}(t) | 0 \rangle + \sum_{n=1}^{\infty} O(e^{-\beta(E_n - E_0)}), \end{aligned} \quad (19)$$

where $|n\rangle$ denotes the state with energy E_n , with E_0 being the ground-state energy. From (19), we see that the corrections from excited states are all very small as long as the temperature is much smaller than the difference in energy between the ground state and the first-excited state, i.e., $\beta(E_1 - E_0) \gg 1$. Therefore, at small temperatures, the thermal OTOC is roughly the same as the ground-state OTOC, and that is why it can also diagnose phase transitions. For more details about the relation between ground-state OTOCs and phase transitions, we refer the reader to [12].

Next, to have a clear understanding of the scrambling properties of our model, we also consider thermal OTOCs of the

form, without time averaging,

$$F_{Z_i Z_j}^\beta(t) = \frac{\text{Tr}[e^{-\beta H} Z_i(t) Z_j(0) Z_i(t) Z_j(0)]}{\text{Tr}[e^{-\beta H}]}, \quad (20)$$

where β is the inverse temperature and H is given by (7). Figure 8 shows the time dependence of $F_{Z_i Z_j}^\beta$ for the system in the QP phase ($s = 0.2$, red curves), and for the system in the F phase ($s = 0.8$, blue curves). In Fig. 8(a), we consider a very small temperature by setting $\beta = 100$. In this case, the thermal OTOC oscillates around a constant value which is close to one (zero) in the QP (F) phase. In Fig. 8(b), we show the results at infinite temperature ($\beta = 0$). In this case, the thermal OTOC oscillates around zero in both phases.

In chaotic systems, thermal OTOCs are expected to approach zero at late times. In our case, thermal OTOCs computed at infinite temperature ($\beta = 0$) display an oscillatory behavior that persists at very large times, oscillating around zero and taking values that roughly range between -1 and 1 ; see Fig. 8(b). The oscillatory behavior around zero is present in both phases of the annealing process and it happens independently of the operator considered in the

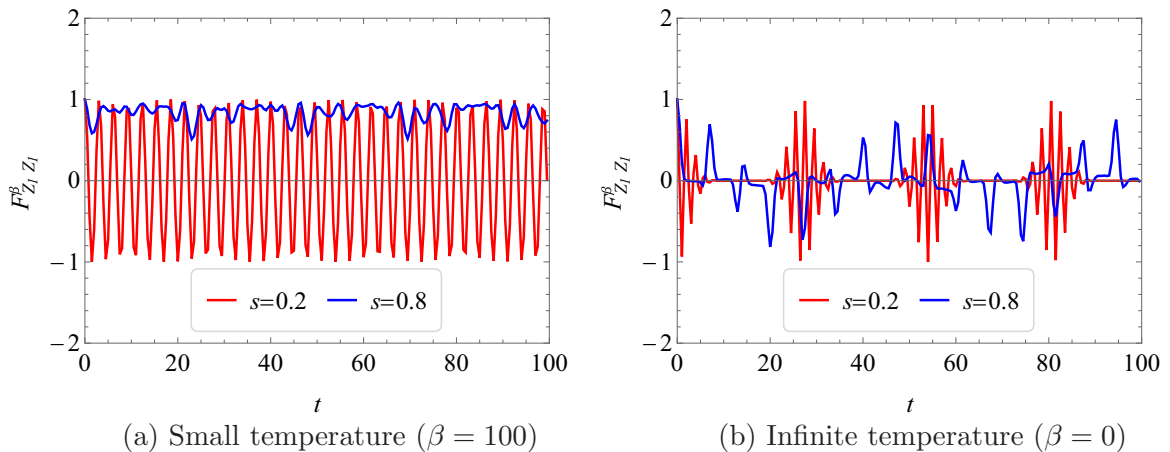


FIG. 8. Time dependence of $F_{Z_i Z_j}^\beta$ for $N = 11$, $p = 5$, and $\lambda = 0.2$. The red curves are for $s = 0.2$ (QP phase) and the blue curves are for $s = 0.8$ (F phase).

OTOC. This should be contrasted with the nonuniversal behavior of ground-state OTOCs $F_{VW}^{(0)}(t)$, which oscillate around a constant value that depends both on the phase and on the operators V and W .

We believe the late-time behavior of thermal OTOCs reflects some kind of weak chaotic behavior in the model (7), which we refer to as *weak scrambling*. The adjective *weak* is because thermal OTOCs do not vanish at late times, as expected in the case of chaotic systems, but only oscillate around zero. We provide a more detailed discussion of the idea of weak scrambling in Appendix A.

IV. LEVEL SPACING STATISTICS

The statistics of the spacing between consecutive energy eigenvalues (level spacing) differs significantly depending on whether we consider chaotic or integrable systems. In chaotic systems, the level spacing statistics obeys a Wigner-Dyson distribution [9], while in integrable systems, it follows an Poisson distribution [10,11]. In the case of systems that are neither integrable nor chaotic, the level spacing distribution usually takes some intermediate form between a Poisson and a Wigner distribution. Several models have been proposed to describe the level spacing statistics of these mixed systems, including, for instance, Refs. [47–51]. In Appendix B, we give more details about the level spacing distribution of mixed

systems. The above statement holds for a properly normalized spectrum, in which the influence of model-dependent density of states is removed through a procedure known as *unfolding*. [52–56].

The Hamiltonian (7) conserves the total spin operator $\mathbf{S}^2 = (S^x)^2 + (S^y)^2 + (S^z)^2$, where $S^x = \frac{1}{2} \sum_{i=1}^N \sigma_i^x$, and so on. We will be interested in the sector with maximal total spin, in which $S = N/2$, where S is the angular momentum quantum number that gives the eigenvalues of the total spin operator, i.e., $\mathbf{S}^2 = S(S+1)$. The reason for that choice is because at the beginning of the annealing process, when $s = 0$, the ground state of H_I has maximal total spin. Since the total spin is conserved during the annealing process, we can restrict our analysis to this subspace.

We use the total-spin basis,

$$\mathbf{S}^2 |S, M\rangle = S(S+1) |S, M\rangle, \quad (21)$$

$$S^z |S, M\rangle = M |S, M\rangle, \quad (22)$$

and, following [29], we label the states as

$$|w\rangle := |S = N/2, M = N/2 - w\rangle, \quad (23)$$

where $w = 0, 1, 2, \dots, N$. In this subspace, the matrix elements of the Hamiltonian $[H]_{\omega, \omega'} := \langle \omega | H(s, \lambda) | \omega' \rangle$ can be written as

$$[H]_{w, w} = s \left[-\lambda N \left(1 - \frac{2w}{N} \right)^p + (1 - \lambda) \left(2w - \frac{2w^2}{N} + 1 \right) \right], \quad (24)$$

$$[H]_{w+1, w} = [H]_{w, w+1} = -(1-s) \sqrt{(N-w)(w+1)}, \quad (25)$$

$$[H]_{w+2, w} = [H]_{w, w+2} = \frac{1}{N} s (1-\lambda) \sqrt{(w+1)(w+2)(N-w)(N-w-1)}, \quad (26)$$

and all other elements are zero.

Here, we study the so-called r -parameter statistics, introduced in [57]. Given a sorted spectrum $\{E_n\}$ and the corresponding level spacing, $s_n = E_{n+1} - E_n$, the r -parameter is defined by

$$r_n = \frac{\min\{s_n, s_{n-1}\}}{\max\{s_n, s_{n-1}\}}. \quad (27)$$

This quantity is independent of the local density of states and so it does not require unfolding. We are interested in the average r -parameter,

$$\tilde{r} \equiv \frac{1}{N-2} \sum_{n=2}^{N-1} r_n, \quad (28)$$

because it takes some simple benchmark values in the case of chaotic systems. For example, $\tilde{r}_{\text{GOE}} \approx 0.53590$, $\tilde{r}_{\text{GUE}} \approx 0.60266$, and $\tilde{r}_{\text{GSE}} \approx 0.67617$, for random matrices of the Gaussian orthogonal ensemble (GOE), Gaussian unitary ensemble (GUE), and Gaussian symplectic ensemble (GSE), respectively.⁵ If the dynamics of a given system is chaotic, one

expects the r -parameter statistics to be described by random matrix theory, and \tilde{r} to take one of the above-mentioned reference values. For integrable systems, one generally expects the statistics of the ratio of consecutive level spacing to be described by a Poisson distribution. In this case, $\tilde{r}_{\text{Poisson}} = 0.38624$. Thus, the average r -parameter \tilde{r} can be used to diagnose the chaotic behavior of the system or the absence of it. It is important to emphasize, however, that in some integrable systems, the level spacing distribution is not described by Poisson statistics. That is the case, for example, of harmonic systems [59]. These deviations from Poisson statistics are usually related to the presence of symmetries that lead to extra degeneracies resulting in commensurability of the spectra [60].

The r -parameter statistics in the case of mixed systems was discussed in [61,62]. In particular, the authors of [62] propose a family of one-parameter distributions that characterizes the r -parameter statistics of systems with different

⁵In the case of 3×3 random matrices, one can show that the distribution of consecutive level spacing ratios $P(r)$ is $P(r) = \frac{1}{Z_\alpha} \frac{(r+r^2)^\alpha}{(1+r+r^2)^{1+\frac{3}{2}\alpha}}$, where $\alpha = 1, 2$, or 4 for GOE, GUE, and GSE, respectively [58]. For a Poisson distribution, $P(r) = e^{-r}$. Here, r denotes a continuous version of r_n . The average r -parameter is defined as $\tilde{r} = \int_0^1 r P(r) dr$.

⁵In the case of 3×3 random matrices, one can show that the distribution of consecutive level spacing ratios $P(r)$ is $P(r) =$

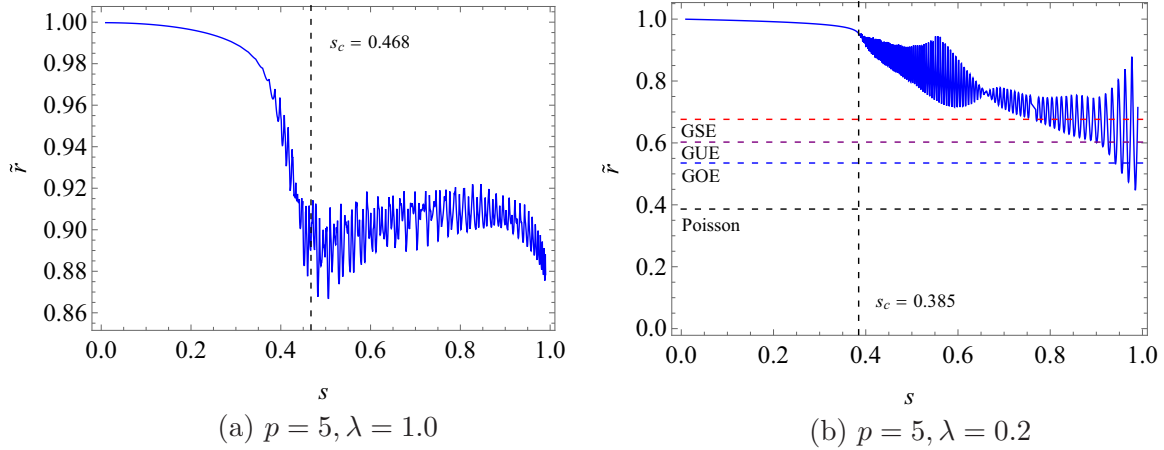


FIG. 9. s dependence of the average r -parameter (\tilde{r}) for the sector with maximal total spin. We set $N = 100$. The red, purple, blue, and black horizontal lines correspond to the value of \tilde{r} for GSE, GUE, GOE, and Poisson distributions. The transition values of s are indicated by a vertical black dashed line. These values agree with our OTOC computation, for example, Fig. 4.

degrees of chaos. The corresponding average r -parameter lies somewhere between $\tilde{r}_{\text{Poisson}}$ and \tilde{r}_{GOE} , \tilde{r}_{GUE} , or \tilde{r}_{GSE} . We give more details about the statistics of spacing ratios of mixed system in Appendix B.

Figure 9 exhibits \tilde{r} for the maximal spin sector of the Hamiltonian (7). For small values of s , \tilde{r} is close to one. As we increase s , the average r -parameter decreases slightly, and it starts to oscillate around the phase transition point. For the antiferromagnetic interactions at $\lambda = 0.2$ [Fig. 9(a)], one can precisely find out the phase transition value of s , which agrees with our OTOC result in Fig. 4(b). After the phase transition, in the F phase, \tilde{r} oscillates wildly as we increase s , taking values that correspond to chaotic behavior for some specific s .⁶ In the case with no antiferromagnetic interactions at $\lambda = 1$ [Fig. 9(a)], one can also estimate the phase transition value of s , which also agrees with our OTOC result in Fig. 4(a), although in this case the phase transition point is less sharp. Moreover, in the F phase, \tilde{r} oscillates around some constant value which is far away from any reference value for \tilde{r} . Thus, in general, our system is neither integrable nor chaotic, being actually a *mixed system*.

Since our system is neither chaotic nor integrable, its r -parameter statistics should be compared with the corresponding spacing ratio statistics for mixed systems. In such cases, the r -parameter distribution usually takes a form that interpolates between a Poisson distribution and a random matrix distribution [62]. In our case, however, we checked that during the annealing process, the r -parameter distribution never resembles the corresponding distributions that are indicative of integrability, chaotic, or mixed behavior. This happens because at the beginning of the annealing process, when $s = 0$, our system is integrable, but it fails to respect the Berry-Tabor conjecture, i.e., its level spacing statistics

⁶For some values of the annealing parameter, \tilde{r} takes the reference values that are indicative of chaotic behavior, so one may think the system may be chaotic for these specific values of s . However, we find that the spacing ratio distribution at these values is not that of the random matrix distributions.

is not described by a Poisson distribution. In fact, at $s = 0$, the system's Hamiltonian reads $H = H_I = -\sum_i^N X_i$, which is basically N times the total magnetization in the x direction. In this special case, the spacing between consecutive energy levels is constant, which leads to an r -parameter distribution completely concentrated in $r = 1$. As we increase the value of the annealing parameter, the distribution gets wider, but it remains concentrated around $r = 1$ until the phase transition point at $s = s_c$. From this point, the peak around $r = 1$ remains, but the distribution also displays nonzero values in the region $r \in [0, 1]$, including additional peaks, which leads to smaller values for the average r -parameter. Therefore, despite the existence of literature about systems with intermediate level spacing statistics, none of these previous works seem to be able to describe the distribution of level spacing ratios of the system under consideration.

It is interesting to question whether the behavior of \tilde{r} versus s can indicate the order of the phase transition. Our result suggests that it may be the case in the sense of the local average value of \tilde{r} over s , \tilde{r}_{avg} , defined as

$$\tilde{r}_{\text{avg}}(s) = \frac{1}{\Delta s} \int_{s-\Delta s/2}^{s+\Delta s/2} ds' \tilde{r}(s'), \quad (29)$$

where Δs is the range of the interval in s that we use to compute the local average. For the second-order phase transition [Fig. 9(b)], the local average $\tilde{r}_{\text{avg}}(s)$ changes smoothly at the transition point, while for the first-order transition, it changes abruptly [Fig. 9(a)].

V. REVERSE ANNEALING AND OTOCS

In this section, we study a relation between reverse annealing and OTOCs. Reverse annealing is a way to find a better classical solution than a given initial solution by starting from an appropriate classical state and gradually increasing and then decreasing the transverse magnetic field [28]. The current D-wave quantum annealer implements reverse annealing and the performance has been studied for various cases [63–65]. Some studies of the efficiency of reverse annealing are provided theoretically [66] and numerically [67], where it is

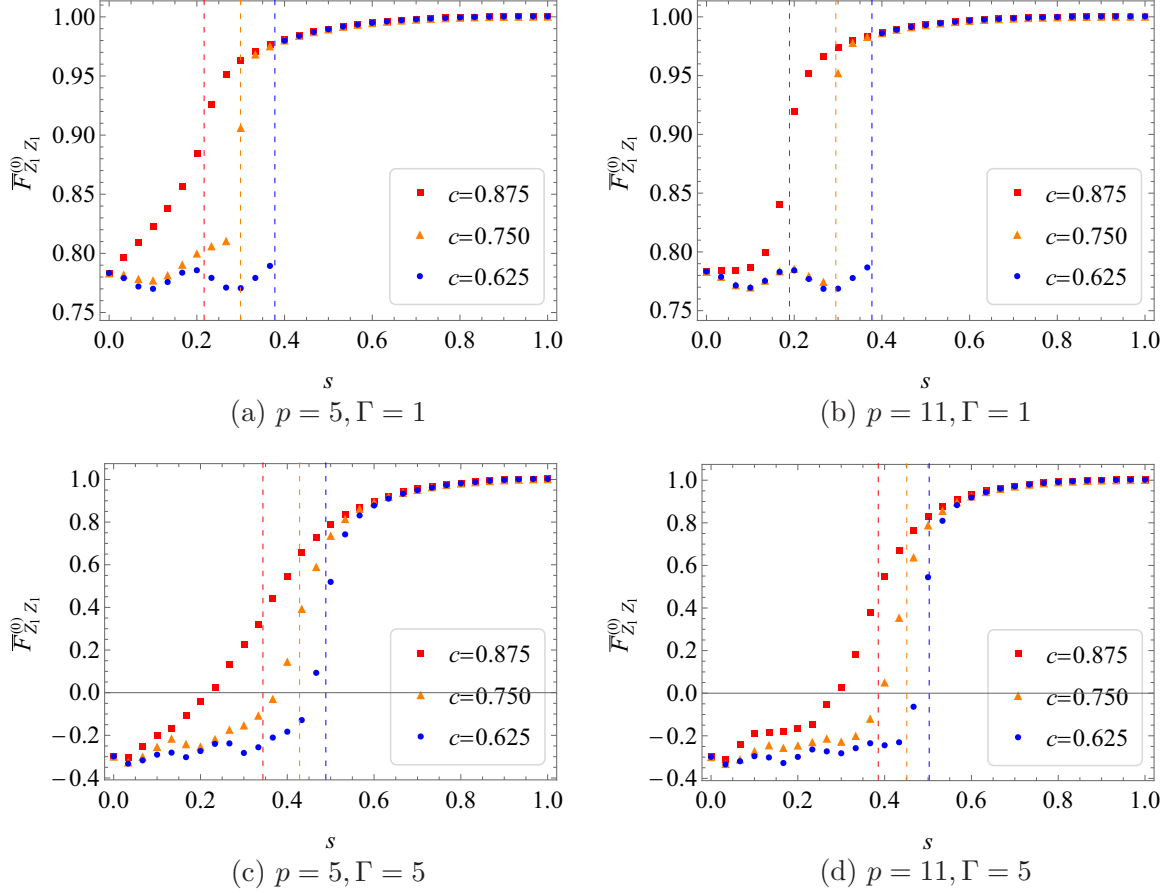


FIG. 10. $\bar{F}_{Z_i Z_i}^{(0)}$ vs s during the reverse annealing process for $N = 8$ and $\lambda = 0.2$. The left panels show the results for $p = 5$, while the right panels show the results for $p = 11$. We set $\Gamma = 1$ in the first row and $\Gamma = 5$ in the second row.

shown that at least for the p -spin model, reverse annealing can turn a first-order phase transition into a second-order phase transition by choosing an appropriate process.

The Hamiltonian of reverse annealing that we will consider is

$$H(s, \lambda) = sH_T + (1-s)(1-\lambda)H_{\text{init}} + \Gamma(1-s)\lambda H_I, \quad (30)$$

where s, λ both take values in $[0, 1]$ and H_T is the Hamiltonian of the p -spin model (4). Γ tunes the strength of the transverse magnetic field H_I (3). H_{init} is the initialization term,

$$H_{\text{init}} = -\sum_{i=1}^N \epsilon_i Z_i, \quad (31)$$

which is $H(0, 0)$ and $\epsilon_i \in \{-1, 1\}$ is the i th component of the given classical initial state. Due to the high spatial symmetry of the p -spin model, without loss of generality we can assign ϵ_i as

$$\epsilon_i = \begin{cases} +1 & \text{for } i \leq N - n \\ -1 & \text{for } i > N - n, \end{cases} \quad (32)$$

where $n \in \{0, 1, \dots, N\}$. The system may be characterized by a parameter $c = 1 - \frac{n}{N} \in [0, 1]$, which is the probability for ϵ_i to be $+1$. The initial magnetization is $2c - 1$. A large c implies that the solution is close to the ground state of H_T . According to [67], the p -spin model experiences phase

transitions by reverse annealing. We will show that the phase transitions can also be detected by OTOCs.

In Fig. 10, we present the time-averaged OTOCs of the form $\bar{F}_{Z_i Z_i}^{(0)}$ as an example. We have confirmed that other choices of operators show the same properties. $\bar{F}_{Z_i Z_i}^{(0)}$ grows around the dotted lines corresponding to the transition points obtained by computing the free energy following Ref. [67]. This confirms that OTOCs can diagnose the phase transition. The smaller c becomes, the larger the transition s becomes. The bigger Γ becomes, the bigger the transition points s become. All these properties are also consistent with Ref. [67]. Furthermore, the curves for $c = 0.625$ (blue circles) suggest a first-order phase transition, while the curves for $c = 0.875$ (red squares) suggest a second-order phase transition. The results for $c = 0.750$ depend on the value of Γ . For $\Gamma = 1$, they suggest a first-order phase transition, while for $\Gamma = 5$, they suggest a second-order phase transition. These are also consistent with Ref. [67] and provide more evidence that time-averaging OTOCs can also diagnose the order of phase transitions. The time-averaging OTOCs may play the role of an order parameter.

VI. CONCLUSIONS AND FUTURE DIRECTIONS

In this work, we have studied quantum phase transitions associated with quantum annealing and reverse quantum annealing for the ferromagnetic p -spin model from the point of

view of quantum chaos. More specifically, we have shown that time-averaging OTOCs and the r -parameter statistics, which are usually used to diagnose quantum chaos, can also be used to diagnose quantum phase transitions.⁷

In the case of quantum annealing (QA), the system's ground state is initially in a quantum paramagnetic (QP) phase ($s = 0$). As we increase the value of s , the system displays a quantum phase transition to a ferromagnetic (F) phase. We observe that the time-averaging OTOC takes an approximately constant value which is different in each phase. The late-time average value of OTOCs of the form $F_{Z_i Z_j}^{(0)} = \langle Z_i(0)Z_j(t)Z_i(0)Z_j(t) \rangle$ vanishes in the QP phase, and it takes a nonzero value in the F phase. In contrast, in the case of OTOCs of the form $F_{X_i X_j}^{(0)} = \langle X_i(0)X_j(t)X_i(0)X_j(t) \rangle$, the late-time average value is nonzero in the QP phase and zero in the F phase. In both cases, despite having different values in each phase depending on the choice of operator in the OTOC, the time-averaging OTOC sharply diagnoses the quantum phase transitions. Time-averaging OTOCs made out of nonlocal operators, $\bar{F}_{S^z S^z}^{(0)}$ and $\bar{F}_{S^z S^z}^{(0)}$, show a qualitatively similar behavior to the local operators $\bar{F}_{Z_i Z_j}^{(0)}$ and $\bar{F}_{X_i X_j}^{(0)}$, respectively.

The operator dependence of $\bar{F}_{VW}^{(0)}$ occurs because we are considering ground-state OTOCs. The ground-state OTOCs are essentially controlled by the properties of the ground state and do not reflect any chaotic property of the ferromagnetic p -spin model. To access the chaotic properties of the model, we need to consider thermal OTOCs at temperatures which are sufficiently larger than the ground-state energy, in such a way that the OTOC receives contributions from excited states. In those cases, however, the thermal fluctuations wash out the special properties of the ground state, and the OTOCs are no longer useful in diagnosing the phase transition. This can be seen in Fig. 7, which shows that the time-averaging thermal OTOCs vanish in both phases at high temperature.

The thermal OTOCs wildly oscillate with time around zero at late times, taking values which range roughly from -1 to 1 ; see Fig. 8. We think this oscillatory behavior reflects two effects: finite-size effects and some sort of weak chaotic behavior. Finite-size effects account for the fact that OTOCs do not vanish at late times in systems whose size is not very large. In fact, it was shown in [42] that for an energy-conserving system, the late-time value of OTOCs scales as an inverse polynomial in the system size. Since our calculation of thermal OTOCs was done for $N \sim 11$, we expect finite-size effects in our results. The second effect, which we call *weak scrambling*, is based on the idea that if the system is not strongly chaotic, or even if it is integrable, the thermal OTOC (for spatially separated operators) will not vanish at late times, but it will rather oscillate around zero, with the size of the oscillation being smaller for systems which are more chaotic. We give more evidence for these ideas in Appendix A using the chaotic Ising model. Similar ideas are also explored in [46].

From the above-mentioned results, we could confirm that time-averaging OTOCs provide useful order parameters to

detect a quantum phase transition, as suggested in [32]. Interestingly, time-averaging OTOCs not only diagnose the phase transition, but they can also distinguish first-order and second-order phase transitions. In the case of first- (second-)order phase transitions, the time-averaging OTOCs display a discontinuous (continuous) behavior at the quantum transition point, just like ordinary order parameters. This suggests that time-averaging OTOCs might be useful in detecting phase transitions when the rigorous order parameter is unknown. Moreover, this works not only for OTOCs constructed out of magnetizations, as observed in [32], but also for quite generic OTOCs made out of local operators. We understand this effectiveness of ground-state OTOCs in detecting phase transitions as resulting from the absence of scrambling (or thermalization) in the ground state, which makes four-point functions sensitive to the symmetries and details of the system, instead of having generic thermal properties. This is based on the assumption that a generic four-point function is able to detect phase transitions, which seems to be the case for the system under consideration.

The effectiveness of ground-state OTOCs in detecting quantum phase transitions motivated us to question if we could also diagnose phase transitions using other probes of quantum chaos. In order to do that, we have studied how the average r -parameter behaves during the quantum annealing process. Figure 9 shows that the average r -parameter clearly changes behavior around the quantum transition point, with the phase transition being sharper in the case with antiferromagnetic interactions ($\lambda = 0.2$). When $\lambda = 1$, the average r -parameter \bar{r} never takes any reference value characterizing random matrix behavior or integrability. In contrast, for $\lambda = 0.2$, the curves of \bar{r} versus s display large oscillations in the ferromagnetic phase, taking values that correspond to chaotic behavior at some specific s . However, we checked that the corresponding level spacing distributions are different from Poisson or random matrix distributions, although sometimes they might have some vague resemblance. Interestingly, the local average of \bar{r} can also distinguish a first- and second-order phase transition like OTOCs. Since we have studied the r -parameter statistics in the maximal spin sector, and the ground state of the system belongs to this sector, it is natural that it can detect the ground-state physics associated to the phase transition. The unusual properties of the r -parameter statistics of the system under consideration result from the fact that at the beginning of the annealing process, the system is integrable, but fails to respect the Berry-Tabor conjecture, having a r -parameter distribution completely concentrated at $r = 1$. The peak around $r = 1$ never disappears across the annealing process, giving a strange form for the r -parameter distribution, which never resembles previously derived distributions for mixed systems [61,62].

In the case of reverse QA, the p -model also displays quantum phase transitions, as shown in [67]. Similarly to the QA case, the time-averaging OTOC also can diagnose the quantum phase transition and its order. There is a quantitative difference from the QA case. In the beginning of the reverse annealing schedule, at $s = 0$, the system already displays a nonzero value of $\bar{F}_{Z_i Z_j}^{(0)}$, which then increases as we increase the values of s .

Finally, we make a comment about the presence of the antiferromagnetic interaction term, H_{AF} , which makes the

⁷Recently, quantum phase transitions from a QP phase into a F phase were observed in a different setup [68]. Our results should be experimentally testable in the same manner.

Hamiltonian nonstoquastic and turns first-order phase transitions into second-order ones during the quantum annealing process. From the analysis of the level spacing statistic, we observe that this term makes the dynamics richer in the ferromagnetic phase. In particular, for some values of s , the system displays some degree of level repulsion, which is typical of chaotic systems. This suggests a connection between chaos and the order of the phase transitions. In particular, it seems that the presence of chaos in the ground-state sector may turn first-order phase transitions into second-order ones. It would be interesting to further investigate this possibility.

ACKNOWLEDGMENTS

We thank Koji Hahimoto, Norihiro Iizuka, Keisuke Fujii, Mikito Koshino, Kin-ya Oda, and Masaki Tezuka for comments and stimulating discussion. We also thank two anonymous referees for insightful and constructive comments on the manuscript. Our collaboration began when the authors attended conferences on strings, particles, and cosmology and on quantum information and string theory. A part of this work was completed when K.I. visited Brookhaven National Laboratory (BNL) and he thanks the members at RIKEN BNL Research Center (RBRC), especially Taku Izubuchi, Dmitri Kharzeev, Yuta Kikuchi, and Akio Tomiya, for hospitality and useful discussion. He also benefited from communication with Akinori Tanaka. K.I. was partly supported by a Grant-in-Aid for JSPS Research Fellows, Grant No. 19J11073. V.J., K.K., and K.H. were supported in part by the Basic Science Research Program through the National Research Foundation of Korea (NRF) funded by the Ministry of Science, ICT and Future Planning (Grant No. NRF-2021R1A2C1006791) and a GIST Research Institute (GRI) grant funded by the GIST in 2021. V.J. was partly supported by the National Research Foundation of Korea (NRF) funded by the Ministry of Science, ICT and Future Planning (Grant No. NRF2020R1I1A1A01073135).

APPENDIX A: INTEGRABLE-TO-CHAOTIC TRANSITION

In this section, we review the time behavior of OTOCs for the Ising model with transverse and magnetic fields,

$$H = - \sum_{i=1}^{L-1} Z_i Z_{i+1} - \sum_{i=1}^L (h_x X_i + h_z Z_i), \quad (\text{A1})$$

where we chose open boundary conditions. The Hamiltonian (A1) is known to display chaotic behavior when $(h_x, h_z) = (-1.05, 0.5)$ [69]. The system is integrable if either h_x or h_z vanish.

We will be interested in the behavior of thermal OTOCs of the form

$$F_{ZZ_j}(t) = \langle Z_i(0) Z_j(t) Z_i(0) Z_j(t) \rangle, \quad (\text{A2})$$

where the expectation value is taken in a thermal state. In Fig. 11, we study the behavior of OTOCs across the integrable-to-chaotic transition that takes place as we change the parameters from the integrable point $(h_x, h_z) = (-1, 0)$ to the strongly chaotic point $(h_x, h_z) = (-1.05, 0.5)$.

Let us first discuss the infinite-temperature results, which are shown in Fig. 11(a). At the strongly chaotic point $(h_x, h_z) = (-1.05, 0.5)$, the OTOC vanishes at late times, which is a signal of scrambling.⁸ As we move away from the strongly chaotic point, the OTOC starts to oscillate around zero, and the amplitude of the oscillations increases as we approach the integrable point. We understand this behavior as a manifestation of *weak scrambling*, in which the OTOCs do not vanish at late times, but rather oscillate around zero, with the amplitude of the oscillations being smaller for more chaotic cases.

The behavior of the OTOCs changes as we reduce the system's temperature. Figure 11(b) shows the results for $\beta = 50$, which are almost the same as the corresponding ground-state OTOCs. Interestingly, the OTOCs at the integrable point $(h_x, h_z) = (-1, 0)$ do not seem to depend on the temperature. For all other values of (h_x, h_z) , the late-time value of the OTOC does not approach zero at late times. Instead, it oscillates around some constant value that depends on (h_x, h_z) . This shows that the OTOC no longer displays universal behavior at small temperatures, and is actually controlled by the ground-state physics. Note that this happens even at the strong chaotic point $(h_x, h_z) = (-1.05, 0.5)$. We understand this phenomenon as an absence of scrambling at low temperatures.

The observed behavior of the OTOCs for the quantum annealing Hamiltonian (7) are qualitatively similar to the ones obtained for the Ising model when we move slightly away from the integrable point, e.g., $(h_x, h_z) = (-1.02, 0.2)$. In both cases, the thermal OTOCs (for sufficiently high temperatures) oscillate around zero, taking some $O(1)$ values. This suggests that the system described by the Hamiltonian (7) is close to being integrable.

Finally, we observe that the phenomenon of weak scrambling bears some resemblance to the idea of *weak thermalization* [69], according to which the long-time limit of local expectation values in certain initial states only converges the thermal value after time averaging. This should be contrasted with *strong thermalization*, in which the instantaneous local expectation value in certain initial states converges to the thermal value in the long-time limit, without the need to consider the time average. Even in a chaotic system, what determines whether or not thermalization happens, or whether it is strong or weak, is the initial state of the system [69]. In particular, it is possible that the ground state of a certain system shows weak thermalization or maybe it does not thermalize at all. This suggests that maybe the absence of scrambling (or chaos) at low temperatures is connected to the absence of thermalization in the ground state of the system under consideration. In fact, it has long been suggested that thermalization in quantum systems is linked to the idea of chaos [70–73]. In particular, quantized chaotic (integrable) systems are (not) expected to thermalize.⁹ Since the system described by the Hamiltonian

⁸Here, by scrambling, we mean the late-time vanishing of OTOCs. In the literature, people sometimes use the term scrambling to refer to the exponential behavior of OTOCs.

⁹The criterium for thermalization in many-body quantum systems is known as the Eigenstate Thermalization Hypothesis (ETH) [71]. See [74–78] for some recent developments involving ETH.

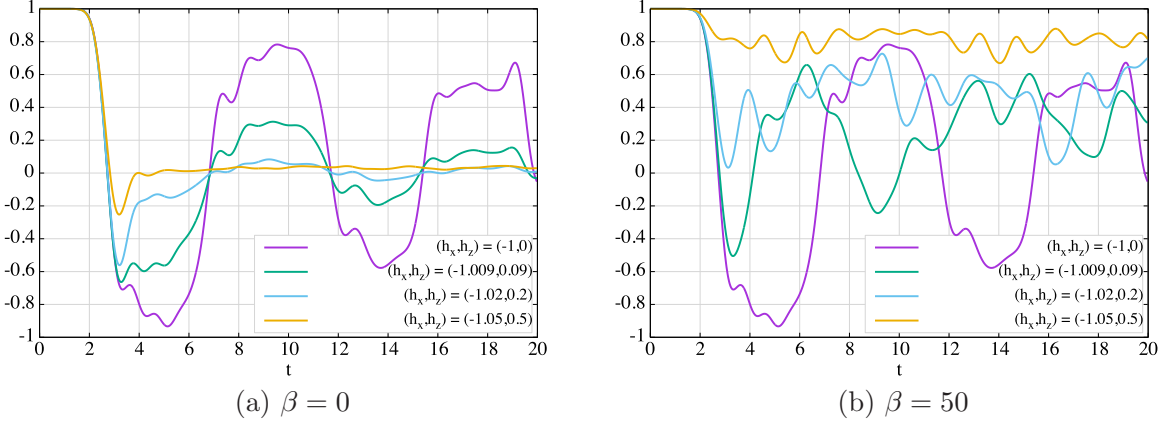


FIG. 11. Thermal OTOCs, $F_{Z_i Z_j}(t) = \langle Z_i(0)Z_j(t)Z_i(0)Z_j(t) \rangle$, for the Ising model with longitudinal and transverse magnetic fields ($L = 8$).

(7) is close to be integrable, we do not expect it to thermalize, especially if the initial state is the ground state. This absence of thermalization leads to the absence of scrambling, which explains why the ground-state OTOCs are sensitive to the ground-state physics and can detect phase transitions, instead of having generic thermal properties.

APPENDIX B: LEVEL SPACING STATISTICS OF MIXED SYSTEMS

The statistics of the spacing between consecutive energy eigenvalues (level spacing) differs significantly depending on whether we consider chaotic or integrable systems. In chaotic systems, the level spacing statistics obeys a Wigner-Dyson distribution [9],

$$P_{\text{WD}}(s) = \frac{\pi}{2} \rho^2 s e^{-\frac{\pi}{4} \rho^2 s^2}, \quad (\text{B1})$$

where $s_n = E_{n+1} - E_n$ is the level spacing associated to a sorted spectrum $\{E_n\}$, and ρ is the mean level density. In contrast, for integrable systems, the level spacing statistics follows a Poisson distribution [10,11],

$$P_P(s) = \rho e^{-\rho s}. \quad (\text{B2})$$

The level spacing distributions (B1) and (B2) can be associated to the corresponding classical motion on a given constant-energy surface [48]. In the case of integrable systems, the orbits are regular, winding round a torus in phase space. For chaotic systems, the orbits are irregular and unpredictable, exploring the entire phase space [48].

In general, the level spacing statistics of generic systems is not described by (B1) or (B2). For the case of systems that have a classical limit, that can be understood as resulting from the fact that their phase space is mixed—some orbits are regular and explore only a fraction of the phase space, while other orbits are chaotic and explore the entire phase space. From now on, we will refer to these systems which are neither integrable nor chaotic as *mixed systems*.

Several models have been proposed to describe the level spacing statistics of mixed systems. The Brody distribution is given by [47]

$$P_B(s) = (\beta + 1) b s^\beta e^{-b s^{\beta+1}}, \quad b = \left[\Gamma\left(\frac{\beta + 2}{\beta + 1}\right) \right]^{\beta+1}. \quad (\text{B3})$$

The Brody distribution reduces to a Poisson distribution for $\beta = 0$ and to a Wigner-Dyson distribution for $\beta = 1$. One shortcoming of the Brody distribution is the fact that it does not have a sound theoretical foundation, being purely empirical.

Another possible way to characterize the level spacing statistics of mixed systems is to use the Berry-Robnik distribution,

$$P_{\text{BR}}(s) = \left[2(1 - \bar{\rho})\bar{\rho} + \frac{\pi}{2} \bar{\rho}^3 s \right] e^{-(1-\bar{\rho})s - \frac{\pi}{4} \bar{\rho}^2 s^2} + (1 - \bar{\rho})^2 \operatorname{erfc}\left(\frac{\sqrt{\pi}}{2} \bar{\rho} s\right) e^{-(1-\bar{\rho})s}, \quad (\text{B4})$$

which interpolates between a Poisson distribution and a Wigner distribution as we change $\bar{\rho}$ from zero to one. The Berry-Robnik distribution can be derived from first principles, by considering the superposition of contributions of level sequences coming from regular as well as chaotic orbits in phase space. Other works characterizing the level spacing distribution of mixed systems include, for instance, [49–51].

Spacing ratio statistics of mixed systems

The r -parameters statistics in the case of mixed systems was discussed in [61,62]. In particular, the authors of [62] propose a family of one-parameter distributions that characterizes the r -parameter statistics of systems with different degrees of chaos. The proposed distribution reads

$$P_{\gamma\beta} = c_\beta \frac{(r + r^2)^\beta}{[(1 + r)^2 - \gamma(\beta)r]^{1+3\beta/2}}, \quad (\text{B5})$$

where β ranges from 0 to ∞ and $\gamma(\beta)$ is a system-dependent quantity.¹⁰ The authors of [62] claim that the above formula can be used to assess the degree of chaos for different symme-

¹⁰For a system displaying a transition from a Poisson to GOE distribution, for example, one has $0 \leq \beta \lesssim 1$ and $\gamma(\beta) = 0.80 - 1.69(1 - \beta) + 0.89(1 - \beta)^5$. The corresponding average r -parameter lies between \bar{r}_{Poisson} and \bar{r}_{GOE} . The ranges of β and the form of $\gamma(\beta)$ change depending on the system and transition under consideration. We refer to [62] for further details.

tries (or mixture of them) under very general circumstances. For mixed systems, one generally expects the average r -

parameter to lie somewhere between $\tilde{r}_{\text{Poisson}}$ and \tilde{r}_{GOE} , \tilde{r}_{GUE} , or \tilde{r}_{GSE} .

-
- [1] A. Larkin and Y. N. Ovchinnikov, Quasiclassical method in the theory of superconductivity, *Sov. Phys. JETP* **28**, 1200 (1969).
- [2] A. Kitaev, Hidden correlations in the Hawking radiation and thermal noise (unpublished), <https://online.kitp.ucsb.edu/online/joint98/kitaev/>.
- [3] J. Maldacena, S. H. Shenker, and D. Stanford, A bound on chaos, *J. High Energy Phys.* **08** (2016) 106.
- [4] V. Jahnke, Recent developments in the holographic description of quantum chaos, *Adv. High Energy Phys.* **2019**, 9632708 (2019).
- [5] B. Yoshida and N. Y. Yao, Disentangling Scrambling and Decoherence via Quantum Teleportation, *Phys. Rev. X* **9**, 011006 (2019).
- [6] M. Gärtner, J. G. Bohnet, A. Safavi-Naini, M. L. Wall, J. J. Bollinger, and A. M. Rey, Measuring out-of-time-order correlations and multiple quantum spectra in a trapped-ion quantum magnet, *Nat. Phys.* **13**, 781 (2017).
- [7] J. Li, R. Fan, H. Wang, B. Ye, B. Zeng, H. Zhai, X. Peng, and J. Du, Measuring Out-of-Time-Order Correlators on a Nuclear Magnetic Resonance Quantum Simulator, *Phys. Rev. X* **7**, 031011 (2017).
- [8] R. J. Lewis-Swan, A. Safavi-Naini, J. J. Bollinger, and A. M. Rey, Unifying scrambling, thermalization and entanglement through measurement of fidelity out-of-time-order correlators in the Dicke model, *Nat. Commun.* **10**, 1581 (2019).
- [9] O. Bohigas, M. J. Giannoni, and C. Schmit, Characterization of Chaotic Quantum Spectra and Universality of Level Fluctuation Laws, *Phys. Rev. Lett.* **52**, 1 (1984).
- [10] M. V. Berry and M. Tabor, Level clustering in the regular spectrum, *Proc. R. Soc. London A* **356**, 375 (1977).
- [11] M. V. Berry, Quantizing a classically ergodic system: Sinai's billiard and the KKR method, *Ann. Phys.* **131**, 163 (1981).
- [12] C. B. Dağ, K. Sun, and L. M. Duan, Detection of Quantum Phases via Out-of-Time-Order Correlators, *Phys. Rev. Lett.* **123**, 140602 (2019).
- [13] Z.-H. Sun, J.-Q. Cai, Q.-C. Tang, Y. Hu, and H. Fan, Out-of-time-order correlators and quantum phase transitions in the Rabi and Dicke models, *Annal. Phys.* <https://onlinelibrary.wiley.com/doi/pdf/10.1002/andp.201900270>.
- [14] Q. Wang and F. Pérez-Bernal, Probing excited-state quantum phase transition in a quantum many body system via out-of-time-ordered correlator *Phys. Rev. A* **100**, 062113 (2019).
- [15] P. Shukla, Level statistics of Anderson model of disordered systems: Connection to Brownian ensembles, *J. Phys.: Condens. Matter* **17**, 1653 (2005).
- [16] P. Shukla, Localization to ergodic transitions: Is Rosenzweig-Porter ensemble the hidden skeleton? *New J. Phys.* **18**, 021004 (2016).
- [17] A. M. García-García, T. Nosaka, D. Rosa, and J. J. M. Verbaarschot, Quantum chaos transition in a two-site SYK model dual to an eternal traversable wormhole, *Phys. Rev. D* **100**, 026002 (2019).
- [18] T. Nosaka and T. Numasawa, Quantum chaos, thermodynamics and black hole microstates in the mass deformed SYK model, *J. High Energy Phys.* **08** (2020) 081.
- [19] T. Nosaka and T. Numasawa, Chaos exponents of SYK traversable wormholes, *J. High Energy Phys.* **02** (2021) 150.
- [20] M. Vojta, Quantum phase transitions, *Rep. Prog. Phys.* **66**, 2069 (2003).
- [21] T. Kadowaki and H. Nishimori, Quantum annealing in the transverse Ising model, *Phys. Rev. E* **58**, 5355 (1998).
- [22] E. Farhi, J. Goldstone, S. Gutmann, and M. Sipser, Quantum Computation by Adiabatic Evolution, [arXiv:quant-ph/0001106](https://arxiv.org/abs/quant-ph/0001106).
- [23] B. Damski and M. M. Rams, Exact results for fidelity susceptibility of the quantum Ising model: The interplay between parity, system size, and magnetic field, *J. Phys. A: Math. Theor.* **47**, 025303 (2013).
- [24] S. Dusuel and J. Vidal, Continuous unitary transformations and finite-size scaling exponents in the Lipkin-Meshkov-Glick model, *Phys. Rev. B* **71**, 224420 (2005).
- [25] P. Pfeuty, The one-dimensional Ising model with a transverse field, *Ann. Phys.* **57**, 79 (1970).
- [26] C. R. Laumann, R. Moessner, A. Scardicchio, and S. L. Sondhi, Quantum Adiabatic Algorithm and Scaling of Gaps at First-Order Quantum Phase Transitions, *Phys. Rev. Lett.* **109**, 030502 (2012).
- [27] J. Tsuda, Y. Yamanaka, and H. Nishimori, Energy gap at first-order quantum phase transitions: An anomalous case, *J. Phys. Soc. Jpn.* **82**, 114004 (2013).
- [28] A. Perdomo-Ortiz, S. E. Venegas-Andraca, and A. Aspuru-Guzik, A study of heuristic guesses for adiabatic quantum computation, *Quantum Inf. Proc.* **10**, 33 (2011).
- [29] Y. Susa, J. F. Jadebeck, and H. Nishimori, Relation between quantum fluctuations and the performance enhancement of quantum annealing in a nonstoquastic Hamiltonian, *Phys. Rev. A* **95**, 042321 (2017).
- [30] G. Passarelli, K.-W. Yip, D. A. Lidar, H. Nishimori, and P. Lucignano, Reverse quantum annealing of the p -spin model with relaxation, *Phys. Rev. A* **101**, 022331 (2020).
- [31] M. Filippone, S. Dusuel, and J. Vidal, Quantum phase transitions in fully connected spin models: An entanglement perspective, *Phys. Rev. A* **83**, 022327 (2011).
- [32] M. Heyl, F. Pollmann, and B. Dóra, Detecting Equilibrium and Dynamical Quantum Phase Transitions in Ising Chains via Out-of-Time-Ordered Correlators, *Phys. Rev. Lett.* **121**, 016801 (2018).
- [33] B.-B. Wei, G. Sun, and M.-J. Hwang, Dynamical scaling laws of out-of-time-ordered correlators, *Phys. Rev. B* **100**, 195107 (2019).
- [34] H. Shen, P. Zhang, R. Fan, and H. Zhai, Out-of-time-order correlation at a quantum phase transition, *Phys. Rev. B* **96**, 054503 (2017).
- [35] R. K. Shukla, G. K. Naik, and S. K. Mishra, Out-of-time-order correlation and detection of phase structure in Floquet transverse Ising spin system, *Europhys. Lett.* **132**, 47003 (2021).
- [36] S. Bravyi, D. P. DiVincenzo, R. I. Oliveira, and B. M. Terhal, The complexity of stochastic local Hamiltonian problems, *Quantum Inf. Comput.* **8**, 0361 (2008).
- [37] Y. Seki and H. Nishimori, Quantum annealing with antiferromagnetic fluctuations, *Phys. Rev. E* **85**, 051112 (2012).

- [38] T. Jörg, F. Krzakala, J. Kurchan, A. C. Maggs, and J. Pujos, Energy gaps in quantum first-order mean-field-like transitions: The problems that quantum annealing cannot solve, *Europhys. Lett.* **89**, 40004 (2010).
- [39] K. Ikeda, Universal computation with quantum fields, *Quantum Info. Proc.* **19**, 1 (2020).
- [40] Y. Ahn, V. Jahnke, H.-S. Jeong, and K.-Y. Kim, Scrambling in Hyperbolic Black Holes: Shock waves and pole-skipping, *J. High Energy Phys.* **10** (2019) 257.
- [41] V. Jahnke, K.-Y. Kim, and J. Yoon, On the Chaos Bound in Rotating Black Holes, *J. High Energy Phys.* **05** (2019) 037.
- [42] Y. Huang, F. G. S. L. Brandão, and Y.-L. Zhang, Finite-Size Scaling of Out-of-Time-Ordered Correlators at Late Times, *Phys. Rev. Lett.* **123**, 010601 (2019).
- [43] V. Khemani, D. A. Huse, and A. Nahum, Velocity-dependent Lyapunov exponents in many-body quantum, semiclassical, and classical chaos, *Phys. Rev. B* **98**, 144304 (2018).
- [44] B. Craps, M. D. Clerck, D. Janssens, V. Luyten, and C. Rabideau, Lyapunov growth in quantum spin chains, *Phys. Rev. B* **101**, 174313 (2020).
- [45] H. Gharibyan, M. Hanada, B. Swingle, and M. Tezuka, Quantum Lyapunov spectrum, *J. High Energy Phys.* **04** (2019) 082.
- [46] E. M. Fortes, I. García-Mata, R. A. Jalabert, and D. A. Wisniacki, Gauging classical and quantum integrability through out-of-time-ordered correlators, *Phys. Rev. E* **100**, 042201 (2019).
- [47] T. A. Brody, A statistical measure for the repulsion of energy levels, *Lett. Nuovo Cimento* **7**, 482 (1973).
- [48] M. V. Berry and M. Robnik, Semiclassical level spacings when regular and chaotic orbits coexist, *J. Phys. A: Math. Gen.* **17**, 2413 (1984).
- [49] G. Date, S. R. Jain, and M. V. N. Murthy, Rectangular billiard in the presence of a flux line, *Phys. Rev. E* **51**, 198 (1995).
- [50] E. B. Bogomolny, U. Gerland, and C. Schmit, Models of intermediate spectral statistics, *Phys. Rev. E* **59**, R1315(R) (1999).
- [51] B. Grémaud and S. R. Jain, Spacing distributions for rhombus billiards, *J. Phys. A: Math. Gen.* **31**, L637 (1998).
- [52] F. Haake, *Quantum Signatures of Chaos* (Springer, Berlin, 1992).
- [53] O. Bohigas and M. Giannoni, Level density fluctuations and random matrix theory, *Ann. Phys.* **89**, 393 (1975).
- [54] A. A. Abul-Magd and A. Y. Abul-Magd, Unfolding of the spectrum for chaotic and mixed systems, *Physica A* **396**, 185 (2014).
- [55] J. M. G. Gómez, R. A. Molina, A. Relaño, and J. Retamosa, Misleading signatures of quantum chaos, *Phys. Rev. E* **66**, 036209 (2002).
- [56] I. O. Morales, E. Landa, P. Stránský, and A. Frank, Improved unfolding by detrending of statistical fluctuations in quantum spectra, *Phys. Rev. E* **84**, 016203 (2011).
- [57] V. Oganessian and D. A. Huse, Localization of interacting fermions at high temperature, *Phys. Rev. B* **75**, 155111 (2007).
- [58] Y. Y. Atas, E. Bogomolny, O. Giraud, and G. Roux, Distribution of the Ratio of Consecutive Level Spacings in Random Matrix Ensembles, *Phys. Rev. Lett.* **110**, 084101 (2013).
- [59] A. Pandey and R. Ramaswamy, Level spacings for harmonic-oscillator systems, *Phys. Rev. A* **43**, 4237 (1991).
- [60] L. D'Alessio, Y. Kafri, A. Polkovnikov, and M. Rigol, From quantum chaos and eigenstate thermalization to statistical mechanics and thermodynamics, *Adv. Phys.* **65**, 239 (2016).
- [61] S. H. Tekur, S. Kumar, and M. S. Santhanam, Exact distribution of spacing ratios for random and localized states in quantum chaotic systems, *Phys. Rev. E* **97**, 062212 (2018).
- [62] Á. L. Corps and A. Relaño, Distribution of the ratio of consecutive level spacings for different symmetries and degrees of chaos, *Phys. Rev. E* **101**, 022222 (2020).
- [63] K. Ikeda, Y. Nakamura, and T. S. Humble, Application of quantum annealing to nurse scheduling problem, *Sci. Rep.* **9**, 12837 (2019).
- [64] D. Venturelli and A. Kondratyev, Reverse quantum annealing approach to portfolio optimization problems, *Quantum Mach. Intell.* **1**, 17 (2019).
- [65] A. D. King, J. Carrasquilla, J. Raymond, I. Ozfidan, E. Andriyash, A. Berkley *et al.*, Observation of topological phenomena in a programmable lattice of 1,800 qubits, *Nature (London)* **560**, 456 (2018).
- [66] M. Ohkuwa, H. Nishimori, and D. A. Lidar, Reverse annealing for the fully connected p -spin model, *Phys. Rev. A* **98**, 022314 (2018).
- [67] Y. Yamashiro, M. Ohkuwa, H. Nishimori, and D. A. Lidar, Dynamics of reverse annealing for the fully connected p -spin model, *Phys. Rev. A* **100**, 052321 (2019).
- [68] X. Nie, B.-B. Wei, X. Chen, Z. Zhang, X. Zhao, C. Qiu *et al.*, Experimental Observation of Equilibrium and Dynamical Quantum Phase Transitions Via Out-of-Time-Ordered Correlators, *Phys. Rev. Lett.* **124**, 250601 (2020).
- [69] M. C. Bañuls, J. I. Cirac, and M. B. Hastings, Strong and Weak Thermalization of Infinite Nonintegrable Quantum Systems, *Phys. Rev. Lett.* **106**, 050405 (2011).
- [70] N. G. van Kampen, *Quantum Chaos as Basis for Statistical Mechanics* (Springer, Boston, MA, 1985), pp. 309–319.
- [71] M. Srednicki, Chaos and quantum thermalization, *Phys. Rev. E* **50**, 888 (1994).
- [72] D. Alonso and S. R. Jain, From random matrix theory to statistical mechanics - Anyon gas, *Phys. Lett. B* **387**, 812 (1996).
- [73] S. R. Jain and D. Alonso, Quantum chaos, random matrix theory, statistical mechanics in two dimensions, and the second law - A case study, *J. Phys. A: Math. Gen.* **30**, 4993 (1997).
- [74] H. Kim, T. N. Ikeda, and D. A. Huse, Testing whether all eigenstates obey the eigenstate thermalization hypothesis, *Phys. Rev. E* **90**, 052105 (2014).
- [75] T. Yoshizawa, E. Iyoda, and T. Sagawa, Numerical Large Deviation Analysis of the Eigenstate Thermalization Hypothesis, *Phys. Rev. Lett.* **120**, 200604 (2018).
- [76] S. Sorg, L. Vidmar, L. Pollet, and F. Heidrich-Meisner, Relaxation and thermalization in the one-dimensional Bose-Hubbard model: A case study for the interaction quantum quench from the atomic limit, *Phys. Rev. A* **90**, 033606 (2014).
- [77] S. Trotzky, Y.-A. Chen, A. Flesch, I. P. McCulloch, U. Schollwöck, J. Eisert *et al.*, Probing the relaxation towards equilibrium in an isolated strongly correlated one-dimensional Bose gas, *Nat. Phys.* **8**, 325 (2012).
- [78] C. Neill, P. Roushan, M. Fang, Y. Chen, M. Kolodrubetz, Z. Chen *et al.*, Ergodic dynamics and thermalization in an isolated quantum system, *Nat. Phys.* **12**, 1037 (2016).